Al Kassas, R, Ross, K, Simm, A, Browning, N, Olier, I and Ting, J

Chitosan nanoparticles for enhancing drugs and cosmetic components penetration through the skin

Chitosan nanoparticles for enhancing drugs and cosmetic components penetration through the skin

Quynh Ta[1], Jessica Ting[1], Sophie Harwood[1], Nicola Browning[2], Alan Simm[2], Kehinde Ross[1], Ivan Olier[3], Raida Al-Kassas[1]*

[1]School of Pharmacy and Biomolecular Science, Faculty of Science, Liverpool John Moores University, James Parsons Building, Byrom St, Liverpool, L3 3AF, UK.

[2]Faculty of Science, Liverpool John Moores University, James Parsons Building, Byrom St, Liverpool, L3 3AF, UK.

[3] School of Computer Science and Mathematics, Liverpool John Moores University, James Parsons Building, Byrom St, Liverpool, L3 3AF, UK.

*Corresponding author:
Dr Raida Al-Kassas
School of Pharmacy and Biomolecular Science,
Faculty of Science
Liverpool John Moores University,
James Parsons Building, Byrom St,
Liverpool, L3 3AF
UK

Abstract

Chitosan nanoparticles (CT NPs) have attractive biomedical applications due to their unique properties. This present research aimed at development of chitosan nanoparticles to be used as skin delivery systems for cosmetic components and drugs and to track their penetration behaviour through pig skin. CT NPs were prepared by ionic gelation technique using sodium tripolyphosphate (TPP) and Acacia as crosslinkers. The particle sizes of NPs appeared to be dependent on the molecular weight of chitosan and concentration of both chitosan and crosslinkers. CT NPs were positively charged as demonstrated by their Zeta potential values. The formation of the nanoparticles was confirmed by FTIR and DSC. Both SEM and TEM micrographs showed that both CT-Acacia and CT:TPP NPs were smooth, spherical in shape and are distributed uniformly with a size range of 200nm to 300 nm. The CT:TPP NPs retained an average of 98% of the added water over a 48-hour period. CT-Acacia NPs showed high moisture absorption but lower moisture retention capacity, which indicates their competency to entrap polar actives in cosmetics and release the encapsulated actives in low polarity skin conditions. The cytotoxicity studies using MTT assay showed that CT NPs made using TPP or Acacia crosslinkers were similarly non-toxic to the human dermal fibroblast cells. Cellular uptake study of NPs observed using live-cell imaging microscopy, proving the great cellular internalisation of CT:TPP NPs and CT-Acacia NPs. Confocal laser scanning microscopy revealed that CT NPs of particle size 530nm containing fluorescein sodium salt as a marker were able to penetrate through the pig skin and gather in the dermis layer. These results show that CT NPs have the ability to deliver the actives and cosmetic components through the skin and to be used as cosmetics and dermal drug delivery system.

Keywords: Chitosan nanoparticles, skin delivery, cosmetics delivery system, skin penetration studies.

TPP or Acacia Chitosan NPs

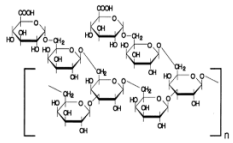

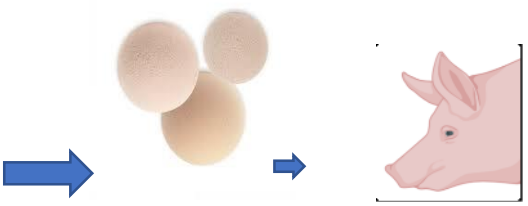

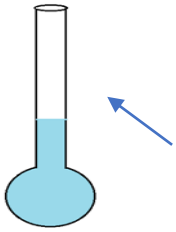

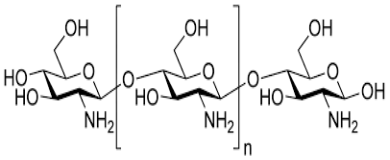

Chitosan

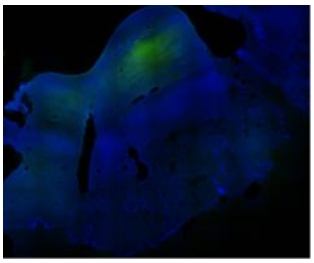

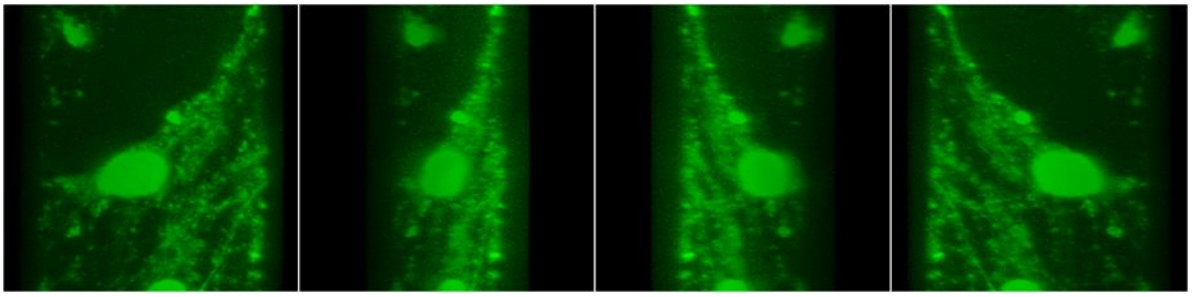

3D images of a single fibroblast cell incubated with CT NPs

1. Introduction

In recent years, nanotechnology has gained widespread attention due to its considerable benefits in the cosmetic industry and drug delivery. Nanotechnology refers to the science and technology carried out at the nanoscale (1 to 100 nm) having applications in the real world and used to develop, monitor and reconstruct matter at the atomic and molecular levels [1]. Nanotechnological approaches entered the field of cosmetics, dermal preparations and other health products nearly 40 years ago with moisturising creams prepared using liposomes [2]. To date, various nanoparticulate delivery systems have been developed for dermal and transdermal drug delivery and most of the studies showed that nanoparticles (NP) enhanced drug penetration into and across the skin [3] and improved the activity and tolerability of the drugs [4]. The nanoparticles (NPs) commonly used as advanced skin delivery systems include polymeric nanocapsules, nanoemulsions. nanocrystals, liposomes, niosomes, micelles, carbon nanotubes, fullerenes, dendrimers, solid lipid nanoparticles and nanostructured lipid carriers.

The effects of NPs on the skin are still a controversial matter among researchers. To illustrate, in terms of skin permeability, some NPs could permeate the outer stratum corneum skin layer, but others were demonstrated to penetrate deeper into the skin layer, even reaching the systemic circulation [5]. There are also some hypothesises showing that NPs might be kept in the skin annexes [6] or skin matrix [7] before penetrating slowly into the deeper skin layer. Accordingly, some characteristics of NPs, including size, charge, shape, and surface properties, need to be studied to evaluate their outcomes on the skin penetration.

Chitosan (CT) is a linear copolymer of b-(1-4)-linked 2-acetamido-2-deoxy-b-d-glucopyranose and 2-amino-2-deoxy-b-d-glucopyranose [8] (Figure 1.a). The polymer is only naturally made by some fungi Mucoraceae [9]. However, it is commercially prepared by the de-N-acetylated of natural polysaccharide chitin (Figure 1). Chitin is the second most plentiful natural biopolymer, mainly found in insect cuticles, the shells of crustaceans and the cell walls of fungi [9]. CT is used widely in topical and transdermal drug delivery systems as a skin permeation enhancer by altering the keratin structure [10]. It acts as a cationic humectant in cosmetics and topical formulations and is absorbed to the negative charges of skin surface. CT tends to improve the water content in stratum corneum and increase the cell membrane fluidity [10]. The hydrophilic hydroxyl groups in CT also contribute to its hygroscopic properties and allow chitosan to interact with the water molecules [11]. The positive charges and relatively high molecular weight promote chitosan adhesion to the skin, supporting its use as a percutaneous drug delivery vehicle. Other attributes that have been reported for CT are antibacterial, antioxidant, anti-inflammatory and UV protective properties [12,13].

The use of CT in the design of NPs as a carrier for active components in cosmetics and drug delivery to skin has gained interest in recent years. CT NPs have been employed for skin drug delivery to treat local disorders such as skin malignant melanoma [14] and infection [15] and for systemic complications such as diabetes [16] and hypertension [17]. Although various studies have been conducted on CT for skin delivery, there is little conclusive evidence that demonstrate that polysaccharide NPs can penetrate epidermis and dermis [18]. Further, the mechanism of polysaccharide NPs in promoting transdermal drug transport is not known. It is not clear if these NPs act primarily as drug release vehicle at skin surfaces, permeation enhancer and drug carrier in skin tissues, or through a combination of actions.

Several techniques have been developed to prepare CT NPs such as ionotropic gelation, polyelectrolyte complexing, emulsification solvent diffusion or micro emulsification [19]. Among these methods, the fabrication of CT NPs by an ionic gelation method is the most favourable one as this method is cost-effective, non-toxic and organic solvent-free. Besides, it provides flexible and easy control for systematically and predictable manipulation of particle size and surface charge [20]. The ionic gelation method relies on the inter and intramolecular linkages between the positively charged primary amino groups in the CT molecule and the negatively charged parts presenting in cross-linkers like sodium tripolyphosphate (TPP), and sodium hexametaphosphate (SHMP). The CT NPs are formed spontaneously upon this interaction. The characteristics of NPs produced by this method might be modified by changing parameters such as temperature, agitation speed, polymer and cross-linker concentrations [21].

Gum Arabic (acacia) (Figure 1.b) is a natural polysaccharide obtained from acacia tree that possess many beneficial effects to the skin and is able to protect against premature skin aging [22]. Acacia is a biodegradable and biocompatible polymer and has been used in oral and topical pharmaceutical products as an emulsifying and suspending agent. Recently, acacia has gained interest in research as a crosslinking agent to CT in ionotropic gelation approach, as it has more interaction sites consisting of negatively charged -COOH groups upon ionization (Figure 1.b) when compared to TPP [23]. As well as CT/TPP NPs, the acacia/CT NPs were found to have positive charges. An observation by Joseph Akinluwade et al., 2018 [24] confirmed the distinct spherical, oval and short cylinder shapes of the CT/acacia NPs. Various formulation parameters have been investigated for production of CT NPs, however studies on the comparison of the effects of different crosslinkers on the characteristics CT NPs are still limited, particularly for producing ideal NPs applied in cosmetics and skin drug delivery.

In this study, we used ionic gelation method to design chitosan nanoparticles for skin delivery to achieve the following aims (1) Optimization of chitosan nanoparticles crosslinked with acacia using factorial design.

(2) Comparison of the effect of two types of crosslinking agents namely acacia and TPP on the physicochemical properties of the developed nanoparticles including particle size, charges, PDI, surface morphology, moisture absorption and retention, cytotoxicity and cellular uptake.
(3) Evaluation of the permeation properties of the chitosan nanoparticles using pig ear skin to track the permeation pathways of the nanoparticles through the skin.

2. Materials and Methods

2.1 Materials

Chitosan differing in molecular weight, low molecular weight (LMW) (50–190 kDa, 75–85% deacetylated), medium molecular weight (MMW) (190–310 kDa, 75–85% deacetylated) and high molecular weight (HMW) (310–375 kDa, > 75% deacetylated) were purchased from Sigma Aldrich (Dorset, UK). Sodium triphosphate pentabasic (TPP), fluorescein sodium salt (FSS), and phosphotungstic acid (PTA) and acetic acid were also obtained from Sigma-Aldrich (Dorset, UK). Acacia, sodium hydroxide, phosphorous pentoxide, and anhydrous sodium carbonate were purchased from Fisher Scientific (UK). All reagents used were of analytical grade.
Human skin fibroblast cells were from University of Cardiff (UK). Gibco™ Dulbecco's Modified Eagle's Medium Media (1X) + GlutaMAX™ -I (DMEM), Gibco® newborn calf serum (NBCS) and Gibco™ Penicillin Streptomycin (Pen-Strep) were supplied by Thermo Fisher Scientific Inc. (USA). Gibco Phosphate-Buffered Saline (PBS) tablets made up to 500mL with distilled water to attain solutions were procured from Life Technologies (UK). Dimethyl sulfoxide (≥99%) (DMSO) was provided by Fisher Scientific (UK). Trypsin-EDTA solution (T), Thiazolyl Blue Tetrazolium Bromide (MTT) and 4',6-Diamidine-2'-phenylindole dihydrochloride (DAPI) were bought from Sigma-Aldrich (USA).

2.2 Factorial Design

This study adopts a 32 factorial design investigating the influence of two independent variables on 3 parameters: particle size, zeta potential and PDI. The independent variables were the concentration of chitosan and the concentration of acacia. A multiple linear regression analysis of the three dependent variables allowed the following equation to be obtained for both factorial designs:

$$Y = \beta 0 + \beta 1x1 + \beta 2x2 + \beta 12x1x2 + \varepsilon$$

Where Y is the dependent variable, β0 is the intercept, β1and β2 are the coefficients of the two independent variables chitosan and acacia, β12 and is the interaction between the dependent variables, ε is error term. Finally, X1 and X2 are the independent variables.

Factorial design was used to optimize the production yield, requiring a minimum of experiments. The influence of the polymer and crosslinker concentrations on the mean diameter (z-AVE), polydispersity index (PdI) and zeta potential (ZP) of the NPs was evaluated using a 32 factorial design , i.e. 2 variables which were set at 3-levels each, with central point for estimating the experimental error requiring a total of 9 experiments. The lower and higher values of the lower and upper levels are represented by (− 1) and (+ 1) and the central point by (0), as summarized in Table 1.

Data were analysed using 'R' version 3.61. An ANOVA test and a Students t-test was performed and findings were considered significant when the p-value was <0.05.

2.3 Preparation of chitosan nanoparticles

Chitosan nanoparticles (CT NPs) were prepared using ionic gelation method. Low, medium or high molecular weight chitosan solutions (0.1%, 0.2% and 0.3%) were prepared in 1% acetic acid, adjusted to pH 4.5 using 0.1M NaOH and filtered to remove any impurities. The crosslinking agents TPP and acacia were dissolved in deionised water at desired concentrations and mixed with an equal volume of chitosan solution under constant stirring. The solution was stirred for 60 minutes before transferring to 10.4 mL polycarbonate centrifuge tubes for ultracentrifugation on a Beckman Coulter Optima XPN-80 (20,000 rpm for 25 minutes at 20°C). The supernatant was discarded, and the pellets were re-dispersed in deionised water and dried on a Buchi Lyovapor L-200 freeze dryer overnight at -20 °C.

2.4 Encapsulation of fluorescein sodium salt (FSS)

The ionic gelation technique was also used to encapsulate fluorescein sodium salt (FSS) into CT NPs. FSS was used as a fluorescent dye to monitor the uptake and distribution of the NPs in the fibroblast cell line. FSS was added to the chitosan solution (10 mL) and sonicated until fully dissolved. The mixture was stirred whilst an equal volume of TPP or acacia was added. After 60 minutes the physicochemical properties such as size, PDI and zeta potential of the FSS-loaded NPs were determined as outlined below.

The content of FSS associated with chitosan nanoparticles was determined on a fluorescence spectroscope (Varian, Inc., California, United States). Samples of FSS-NPs (8 ml) were centrifuged in an Optima XPN-80 ultracentrifuge (Beckman Coulter Inc., Brea, California, USA) at 20,000 rpm for 20 minutes or 49192 G force (Relative Centrifugal Force). The supernatant was diluted 30-fold and measured at an excitation of 460 nm, emission of 515 nm. The concentration of FSS was calculated based on a calibration curve of free FSS constructed by fluorescence spectroscopy with R^2 = 0.9812. Each sample was measured three times. The encapsulation efficiency was calculated according to equation (2.1).

EE (%)= (Initial amount of added FSS-Amount of free FSS)/(Initial amount of added FSS) x 100 (2.1)

2.5 Particle Size and Zeta Potential measurements

A Malvern instruments ZEN3600 ZetaSizer (Mal 1096674) was used to measure the particle size, polydispersity index (PDI) and zeta potential. For analysis of particle size and PDI, a 4 clear-sided cuvette was used with the laser at a scattering angle of 173°. The Zeta Sizer was set to run 3 times per sample, with 10 sets of 5 second measurements in each run. Zeta Potential was measured using a Malvern folded capillary cell with 3 runs of 10 measurements per sample. An average of these measurements was taken for each sample.

2.6 Fourier-Transform Infrared Spectroscopy (FTIR)

Samples were analysed using an ATR-FTIR (Agilent Technologies Cary 630) operating from 4000-650 cm-1 with a resolution of 8 cm-1, programmed by MicroLab FTIR software. To reduce interference, a background scan was performed, and the crystal was cleaned using isopropanol before loading and close pressing the samples. The FTIR was used to produce spectra of chitosan, TPP, acacia, a 1:1 physical mixture of chitosan and TPP, a 1:1 physical mixture of chitosan and acacia, freeze dried nanoparticles containing TPP and freeze-dried nanoparticles containing acacia.

2.7 Differential Scanning Calorimetry (DSC)

Thermal transition properties of the samples were analysed using a Perkin Elmer DSC 7 equipped with a refrigerated cooling system and controlled by a Perkin-Elmer thermal analysis controller TAC 7/DX. A sample weighing between 3 and 8 mg was first crimped in the Perkin-Elmer aluminium pan with a cover by using a Standard Sample Pan Crimper Press and loaded into the DSC. The DSC was set to heat from 25°C to 350°C at 10°C min-1, under a nitrogen purge of 20 mL min-1.

2.8 Morphological studies

The nanoparticles morphology was evaluated using scanning electron microscopy (SEM) and transmission electron microscopy (TEM). For particles evaluated by SEM, the freeze-dried particles were sprayed with gold and imaged on a FEI Quanta 250 SEM to establish their morphology. A Morgagni 268D TEM was used to analyse the morphology of nanoparticles in suspension. The TEM samples were prepared by staining the nanoparticle with 1% Phosphotungstic acid (PTA)solution then placing the stained nanoparticles on a copper grid coated with a formvar film. The grid was left to air dry then transferred to TEM for imaging.

2.9 Moisture Absorption

The freeze-dried NPs (50 mg) were transferred into a desiccator containing saturated sodium carbonate solution which provided a relative humidity (RH) of approximately 43% and left at room temperature for 48 h. The moisture absorbance (Ra) was calculated using the following equation:

$$Ra\ (\%) = 100\ x\ \frac{(Wn - W0)}{W0}$$

Where Wn andW0 refer to the final and initial weight of the sample respectively. The samples were weighed at set intervals over 48 h. This was performed in triplicate for both TPP and acacia nanoparticles.

2.10 Moisture Retention

The freeze-dried nanoparticles (50mg) were moisturised by adding 10% deionised water (5µL) then transferred into a desiccator containing phosphorus pentoxide. The experiment was left at room temperature for 48 h. The moisture retention (Rh) was calculated using the following equation:

$$Rh\ (\%) = \ 100\ x\ \frac{(\mathrm{Hn})}{(H_0)}$$

Where Hn and H0 refer to the final and initial weight of the sample respectively. The samples were weighed at set intervals over 48 h. This was performed in triplicate for both TPP and acacia nanoparticles.

2.11 Cell Viability Assay

The effect of the CT NPs on human dermal fibroblasts (HDFs) was determined using the 3-(4,5-Dimethylthiazol-2-yl)-2,5-diphenyltetrazolium bromide (MTT) assay which is a colourimetric assay [21]. Immortalised HDFs, a kind gift from Professor Phil Stephens (University of Cardiff, UK), were maintained in Dulbecco's Modified Eagle's medium with GlutaMax, penicillin/streptomycin antibiotics, 10% newborn calf serum (NBCS), all of which were purchased from Thermo Fisher Scientific (Paisley, UK). The HDFs were seeded in 96 well plates at 10,000 cells/well in the presence of 200 µL complete growth medium. After 24 h, the medium was replaced with 200 µL of NP samples prepared in serum-free media with 10% (v/v) acetic acid (pH 4.5) and 1%, 3%, 5% and 10% (v/v) of MMW CT NPs suspension, respectively. After 48 h, 20 µL of MTT stock solution (5 mg/ml) was added to each well and incubated for 3-4 hours. The MTT solution was discarded the formazan crystals solubilised in. 100 µL of DMSO under the dark conditions. The optical density of the formazan product was determined at 570 nm on an Epoch Microplate Spectrophotometer (BioTek Instruments Ltd., Swindon, United Kingdom). Cell viability was expressed as a percentage of absorbance relative to a control after background subtraction.

2.12 Cellular Uptake Study

The HDFs were seeded at 2.5x10^5 cells 35 mm round glass coverslips for 24 h, after which the media was replaced substituted with 1 mL of fresh medium containing: FSS, FSS loaded NPs-TPP and FSS loaded NPs-acacia, which each contained 25 ng/mL of FSS. The cells were incubated at 37°C for 3 h and washed three times with ice-cold phosphate-buffered saline. Subsequently, they were covered with ice-cold 100% methanol for fixation at -20°C for 15 minutes, washed in PBS (3 times, 5 minutes each) and stained with 4′,6-Diamidine-2′-

phenylindole dihydrochloride (DAPI). The samples were observed on a Leica DMI6000B fluorescence microscope at excitation wavelengths of 460 to 500 nm and emission wavelengths of 512 to 542 nm or on a Zeiss confocal laser scanning microscope (LSM 7 10, Carl Zeiss, Oberkochen, Germany) at excitation wavelengths of 488 nm and 405 nm for FSS and DAPI, respectively.

2.13 Porcine Skin penetration study

Porcine ear skin was obtained from a local butcher and frozen at -20°C. The ear was defrosted at room temperature, cleansed under the running tap water and dried with cotton tissue before use. A scalpel was used to cut 1.5x1.5 cm sections of the skin and FSS CT NPs (100µL) was massaged into the sections for 5 minutes. The treated porcine ear block placed inside a desiccator containing saturated sodium carbonate solution (RH≈43%) was incubated in an incubator set at 32 °C for 3 h. The frozen samples were cryosectioned to the thickness of 50µm using Leica CM3050 S Research Cryostat. Tile scan images of the cryosectioned tissue were visualised using a Leica DMI6000B fluorescence microscope using the green (GFP/FITC) filter cube. Ex filter BP 480/40 Emission filter: BP 527/30. The images captured were analysed for intensity line profile by Fiji Image J.

2.14 Statistical Analysis

The data were analysed statistically using one-way ANOVA (SPSS version 26, SPSS Inc., Chicago, USA). Statistically significant differences were assumed when $p < 0.05$. All values are expressed as their mean ± standard deviation.

3. Results & Discussion

3.8 Optimization of chitosan : acacia nanoparticles using 3^2 Factorial design

The development of a new formulation requires studying various variables which needs to be considered when incorporating a new API. Designing a factorial study allows saving on resources and sample size when compared to designing three separate parallel group studies for each experimental treatment**.** From an experimental point of view, optimising experiments on nanoparticles development is useful to save time and scientific resources. Thus, factorial experimental designs are used to optimise the experiments and identify which factors affect the experimental outcome, and the extent of which these factors bring a better response.

In this study, CT NPs crosslinked with acacia were studied and optimized by a factorial design. The study adopted a 3^2 factorial design investigating the influence of two independent variables on 3 parameters: particle size, zeta potential and PDI. The independent variables selected for the study were the concentration of chitosan (X1) and the concentration of acacia (X2) (Table 1).

The formulation with 1:1 chitosan to acacia ratio was chosen as the first formulation to allow clear interpretation of data. As shown in Table 2, the nanoparticle size increased with

increasing concentrations of chitosan and acacia. Although both chitosan and acacia concentrations demonstrated effect on nanoparticles size, the chitosan concentration caused a bigger influence than the acacia concentration. There are a few factors that cause an increase in nanoparticle size with the concentrations. The solution viscosity tends to increase when the chitosan concentration increases, and larger nanoparticles will be formed upon cross-linking process. A higher acacia concentration did not show an obvious increase in viscosity and therefore it had less impact on the particle size. Besides that, higher chitosan concentration results in an increased amount of chitosan deposits on the surface and eventually enlarges the nanoparticles. Balance between the electrostatic repulsion and hydrogen bonding is also one of the factors affecting the nanoparticle sizes. The protonation of amino groups in chitosan developed under acidic conditions will result in the presence of electrostatic repulsion and hydrogen bond interactions between chitosan molecules. Therefore, higher chitosan concentration will promote protonation and eventually increase the size of nanoparticles.

Zeta potential (ZP) implies the surface charge characterisation of the nanoparticles and also quantifies their charge stability. Neutralisation occurs when positively charged amine groups in chitosan react with negatively charged acacia gum in the ionic gelation mechanism. This possibly explains that the chitosan-acacia nanoparticles yielded are all positively charged. The magnitude of ZP also demonstrates the stability of nanoparticles suspension. The nanoparticles are more stable at a higher magnitude due to increased electrostatic repulsion. All CT:AC NPs produced in this study are positively charged in the range from +27.8mV to +41.9.7 mV, which was attributed to the positive charge of the CT, as shown in Table 2 and which further confirming the stability of the formulations. High positive values of ZP can reflected in luck of aggregation of investigated nanoparticles, and thereby stabilize their dispersion [25]. The polydispersity index (PDI) indicates the dispersion homogeneity with the value range from 0 to 1, in which the values closer to zero suggest a homogenous dispersion while the values above 0.5 suggest high heterogeneity. All the experimental PDI results obtained are below 0.5 and this implies that the dispersion is relatively homogenous.

Student's t-test was performed for each of the three dependent variables or parameters to determine the significance of the effects and their interaction, and results obtained are presented in Table 3. Any p-value smaller than 0.05 is considered as statistically significant. From the table, it can be seen that Acacia (β2) and its interaction with Chitosan (β1) are relevant predictors for ZP, but not Chitosan (β1) itself. However, almost the opposite is observed for Z-Ave: Chitosan was the only relevant predictor. For PDI, none of the predictors are statistically significant,

Additionally, ANOVA analysis was performed to test overall regression model significances. Results for the three models can be seen in Table 4, one for each parameter. Obtained p-

values were significantly smaller (<0.001) for all parameters, which indicates that their regression models are statistically different from a null model with no predictor factor. This also confirmed with the F-statistic values, as they are far from zero. In addition, multiple and adjusted R-squared values are greater than zero for all parameters, whilst residual standard errors are low. The response plots presented in Figure 2 also shows that the zeta potential is strongly depending on the chitosan and acacia concentrations, followed by polydispersity index and the nanoparticle size.

3.2 Effect of chitosan molecular weight and type of crosslinker on particle size and zeta potential measurements

One of the objectives of this study was to investigate and compare the influence of the type of cross-linking agent and chitosan MW and on the on nanoparticles characteristics and results are presented in Table 5. Two types of cross linkers were studied, acacia and TPP. Particle sizes of NPs formed by LMW chitosan and TPP are approximately 200 nm, but those fabricated by LMW CT and acacia were much higher, around 250 nm. Similarly, in the case of MMW CT, NPs produced from acacia (284.37±3.6) were larger than those prepared using TPP (251.57±13.74) (Table 5). However, the average sizes of HMW CT NPs/acacia are significantly lower than HMW CT NPs/TPP. The gap in particle sizes among NPs prepared by CT at three levels of MW and TPP appeared to be broader than that by acacia. Table 5 also indicated that for both two crosslinkers, the average NPs sizes were affected by CT MW, as they seemed to have a rising trend with the increase in MW of CT. These results are in agreement with previous findings concluding that particle sizes of CT NPs are dependent on CT MW (R [26, 27]. This can be attributed to longer chains of polymers, forming more massive particles.

Regarding the polydispersity index, all three types of chitosan NP formulated with TPP formed highly heterogeneous NPs suspension, reflected in high average PDI values (≥ 0.49), especially HMW chitosan (0.79±0.36). In contrast, NPs produced by CT and acacia have lower PDI results, which were from 0.25 to 0.35, suggesting the formation of homogenous dispersion. All CT NP samples have positive values of zeta potential shown in Table 5, confirming that they are positively charged. To be more specific, chitosan structure is rigid crystalline as a result of its inter- and intramolecular interaction by hydrogen bonding. The electrostatic charge repulsion between the chains accounts for the more extended and flexibility of the molecules in aqueous solutions. When interacting with negatively charged cross-linkers, chitosan can spontaneously provide nano complexes with an overall positive surface charge. NPs formed by MMW chitosan and TPP (33.77±0.96) or acacia (32.87±0.98) show higher zeta potential values than NPs formed by LMW chitosan with TPP or acacia. Nevertheless, HMW chitosan provided NPs having surface charge even lower than LMW chitosan when combining with TPP. It differs from a conclusion stated by Rampino et al. (2013)

[26] that CT samples at different MW should have dissimilar accessibility to cationic groups; thus polymers with a longer chain led to a higher surface charge for NPs. As zeta potential of CT NPs increased linearly with a rise in CT concentration [20], the decrease of the HMW chitosan concentration could be due to the poor solubility of the polymer might have reduced the intensity of NPs surface charge.

3.3 Fourier-Transform Infrared Spectroscopy (FTIR)

Chitosan, TPP and acacia, physical mixtures of chitosan and the crosslinkers and freeze-dried NPs were analysed for their structural components using FTIR. FTIR spectrum analysis of chitosan, Table 6, shows the overlapping O – H stretch and N – H stretch at 3345cm-1. The band at 2864cm is characteristic of the C – H stretching vibration. The bands at 1653 and 1589cm-1 indicate vibrations of the C = O stretch and N – H bend of amide I and amid ll, respectively. ~~The band at 1420 is attributed to asymmetric deformations of C-H group of acetamide remaining in the~~ polymer chain, as the chitosan is not completely deacetylate. The band at 1377cm-1 is characteristic of the C – H deformation bending vibration. The characteristic band at 1149cm-1 attributed to the C – N stretching vibration of the amide groups. Finally, the bands at 1023 and 1058cm-1 indicating the C – O stretching vibration associated with the skeletal structure of chitosan.

Spectrum of TPP, Figure 3, contains a band at 1209cm-1 which indicates P = O stretching vibration. The band at 1136cm-1 is characteristic of O – P = O symmetric and asymmetric stretching vibration. Lastly, the band at 1095cm-1 is attributed to the symmetric and asymmetric stretching vibration of the PO3 groups, where the band at 889cm-1 is typical of P – O – P bridge asymmetric stretching vibration. All of which are structural components of TPP. Comparing the spectrum of chitosan to that of the NPs, there was a shift in the bands 1653 and 1589cm-1 to 1636 and 1541cm-1 which indicates an ionic interaction between chitosan and TPP. This is essential in the formation of the nanoparticles. A wavenumber at 1541cm-1 is indictive of N-O-P stretching vibration of the bond formed between the P-O- of TPP phosphate groups and +NH3 within the chitosan chain, to form the nanoparticle membrane. In comparison, this band was absent (or maybe shifted) from the spectra of the physical mixture of chitosan and TPP in Figure 3, supporting the conclusion that this band results from the interaction between the two components. This, along with an increase in intensity of these peaks, has been observed in other work [28-30].

From the acacia spectra, O – H stretching attributing to the characteristic of glucosidic ring occurred at 3257 cm-1 whereas C – H stretching occurred at 2886 cm-1 [3]. Two characteristic absorption bands were also observed; O=C-O bond was stretching symmetrically at 1595 cm-1 whereas the carboxylic ion axial was stretching asymmetrically at 1407 cm-1[31, 32]. A broad absorption band was observed at 1023 cm-1 and this suggested the presence of C – O

– H stretching [31]. According to literature, a fusion absorption peak resulting from the O – H stretching vibration and N – H stretching vibration was detected near 3306 cm-1 of the nanoparticles spectra [31]. A hydrocarbon group was also observed in the freeze-dried nanoparticles at 2918 cm-1 [31, 3]. Furthermore, overlapping of the COO- main stretching in acacia and the charged amino (NH3+) asymmetrical bending in chitosan was investigated in between 1400 and 1600 cm-1 [31,3]. The absence of usual amino band from the chitosan spectra explains the interaction between cationic chitosan and anionic acacia.

3.4 Differential Scanning Calorimetry (DSC)

Chitosan, the two crosslinking agents, physical mixtures of chitosan and the crosslinkers and freeze-dried nanoparticles were analysed by DSC to compare the thermal transitions (Figures 4a&b). The DSC curve of chitosan shows an endothermic event at 90°C, which is due to the loss of bound water [32]. There is also an exothermic event at 320°C which is likely to be due to decomposition of chitosan. These events are also shown in other researches [33, 34]. TPP showed a slight endothermic peak at 200°C [35].

CT:TPP NPs thermograph exhibited an endothermic event from 90 -120°C which differs from the thermograph produced by a physical mixture of chitosan and TPP. This could be water evaporation from the sample. This peak implies the formation of a new structure between chitosan and TPP i.e. the ionic interaction formed between the positive amide groups of chitosan and the negative phosphate groups of TPP as this peak is not present in the other thermographs shown in Figure 4.a.

From the thermo-grams shown for both acacia and chitosan, an endothermic peak was demonstrated between 80 °C and 90 °C. Meanwhile, the 1:1 physical mixture and the freeze-dried NPs showed their narrower endothermic peaks around 75 °C. These peaks are also known as dehydration temperature that indicate the evaporation of residual water presented in the samples.

3.5 Morphological assessment

The CT:AC and CT:TPP NPs presented as spherical shapes with a smooth surface and are in uniform distributions (Figure 5.a) and form aggregates. The figures confirm the mean size which are likely to be in the size range from 200 to 300 nm. The wet nanoparticles imaged by TEM (Figures 5.b) are also presenting spherical shapes with a smooth surface and in size range of 200-300 nm.

3.6 Moisture absorption and retention

The moisture absorption properties at RH 43% was investigated and compared for both CT:AC and CT:TPP NPs. As shown in Figure 6.a, both of CT:AC and CT:TPP NPs absorbed the moisture rapidly and reached the peak in the first hour. However, the nanoparticle samples started to lose moisture after an hour and rate of moisture loss was higher for CT:TPP than that for CT:AC NPs. The moisture content was level from 3 to 7 h, increased at 24 h to 11%,

then dropped then increased again gradually from 26 h to 48 h to reach a value of 14.5%. The fluctuation of moisture level observed for the nanoparticles can be explained by the high partial pressure of saturated vapour at the initial stage of the experiment led to high absorption activity of the particles. At some stage, there seems to be a “boost” in moisture content probably due to the very high difference in pressure between the nanoparticles and the water surroundings at the initial stage of water sorption activity [36]. The rate of water sorption declined as the moisture content in the particles increased [37]. In general, moisture content of the NPs reached a plateau when the moisture content of the nanoparticles became in equilibrium with the relative humidity surrounding the NPs. From figure 6.a it can be concluded that CT:AC NPs possess better absorption capacity than the CT:TPP NPs which could be due to the additional effect from presence of acacia.

both NPs have high moisture-retention ability and that both released water slowly (Fig. 6b). However, the moisture retention ability was higher for CT:TPP than that for CT:AC nanoparticles, but the difference was not marked. Hygroscopicity is a relatively important factor for the moisture absorption capacity of the polymeric nanoparticles. Chitosan has a strong hygroscopic nature with great capability of forming hydrogen bonds with water [38]. One study conducted on chitosan water sorption under the environment providing 60% RH at room temperature demonstrated that chitosan absorbed 14% to 16% w/w of water within 100 minutes [38]. This analysis is similar to the results obtained from the experiment; CT:AC and CT :TPP NPs absorbed 16.171% w/w and 14.1% of water in average within 60 minutes. This proved that acacia and TPP did not limit the moisture absorption capacity of the freeze-dried nanoparticles.

The main purpose of moisturisers introduced in cosmetics and topical formulations is to maintain the skin’s moisture. Humectant is one of the moisturizer subcategories and it is used in cosmetics to replace natural moisturising factors (NMFs) that present in the skin keratin layer [39]. The moisture absorption capacity of chitosan nanoparticles observed in this experiment reflect their abilities to hydrate the stratum corneum by attracting water from the external environment.

3.7 Cell viability assay

The evaluation of the effects of NPs on human cells provides crucial evidence to support their safety for healthcare applications [11]. In this study, the safety of CT NPs suspension towards the skin was assessed on immortalised HDFs, which account for the primary cell type in the skin dermis layer. Their functions are to synthesis and remodel the extracellular matrix proteins, forming connective tissue and supporting cutaneous wound healing. There have already been some studies on the cytotoxicity of CT NPs against HDFs; however, there is lack of investigations on the effects of crosslinkers on the cell viability of CT NPs.

The viability of HDFs exposed to CT NPs suspension was evaluated using the MTT assay, which relies on the reduction of MTT by mitochondrial dehydrogenase in live cells to form purple formazan crystals [40]. Cell viability declined only slightly as the concentration of CT NPs suspensions increased, regardless of the cross-linker used (Figure 7). The minimum of around 80% viability was recorded after 48 h treatment ($p < 0.05$). Therefore, at the concentration ranging from 1% to 10%, CT:TPP and CT:AC NPs suspensions appear not to exhibit cytotoxicity against FCs. Also, cell viability of CT:TPP NP suspension was slightly lower than that of CT:AC NP suspension from the concentration of 3% to 10% ($p < 0.05$). CT NPs are positively charged, which can adhere to the cell membrane, disrupting the cell [11]. However, the zeta potentials of CT:AC NPs and CT:TPP NPs were very similar (32.87±0.98 vs 33.77±0.96, respectively), hence no difference in their effects on cell viability.

With high cell viability results at the concentration from 1% to 10%, the two types of MMW CT NP suspension were concluded to be safe on human dermal fibroblast cells (FCs), despite the adverse effects of acetic acid and potential toxicity generated by nano-objects [41]. It agrees with the non-toxic, biocompatible and biodegradable properties of all components forming the NPs including chitosan, TPP and acacia.

3.8 Encapsulation of fluorescein sodium salt (FSS) into chitosan nanoparticles and cellular uptake study

Fluorescein sodium salt (FSS) was encapsulated into both CT:TPP and CT:AC NPs. The entrapment efficiency (EE) was 90.42 ± 0.12% for TPP crosslinked NPs and 86.30 ± 0.10% for acacia crosslinked NPs. The zeta potential measurements were 23.5 ± 1.80 for CTTPP NPs and 38 ± 3.38 for CT:AC NPs. The particle size were 304.10 ± 12.56 nm for CT:TPP NPs and 576.87 ± 29.89nm for CT:AC NPs which were higher than the size drug free NPs. The results confirm that FSS was effectively loaded in CT NPs.

The cellular internalisation of the CS NPs was analysed by the live-cell imaging microscopy (LCIM) and confocal microscopy, using FSS as a readily detectable marker. FSS was internalised by HDF as both two NPs samples were visible in over 80% of cells (Figures 8 a & b). Internalisation was confirmed by, the z-stack image series of a single cell incubated with CT NPs recorded by the confocal microscope (Figure 8.c&d) depicted that the fluorescent intensity through the cytoplasm. The uptake of FSS encapsulated in both CT/TPP NPs and CT:AC NPs by FCs is asserted to be productive and confirmed by the strong fluorescent intensity. The small size of both nanoparticles has contributed in their entering and translocation across the cells easily [41].

3.9 Skin penetration study

Human skin and porcine skin show similarity in terms of skin attachment, hair coat, epidermis thickness, dermis thickness, presence of panniculus carnosus, and healing mechanism [43]. Therefore, porcine ear skin was used as a model for human skin to analyse the ability of the

CT NPs to penetrate skin. A study has presented the comparison between the skins of different species including guinea pig, human, mouse, pig, and rat [43].

One of the cryosectioned biopsies of treated porcine ear skin was visualised and the tile-scanning image (Figure 9.a) was captured. In order to determine the distance of porcine ear skin penetration, a line from position A to B was drawn on the image taken (Figure 10.a) by using ImageJ in order to generate a profile based on the grey value and the permeation distance (Figure 9.b). The intensity of grey value reflects the distance of permeation in micrometer (μm) and the distance between A and B calculated by ImageJ is approximately 2500 μm. The fluorescein sodium encapsulated nanoparticles penetrated the porcine ear skin to the furthest distance of around 1900 μm. The highest grey value interpreted from Figure 10.b. is 45.8 and its skin penetration distance displayed is at 629μm. This result indicated that these nanoparticles have the potential to penetrate into the dermis layers and likely to the subcutaneous layers.

4. Conclusion

Ionic gelation of chitosan with two crosslinking agents (TPP and acacia) tends to yield nanoparticles with particle sizes depending on the CT MW and concentrations of chitosan and TPP or acacia. This approach is easy and reproducible in formulating positively charged spherical nanoparticles with a smooth surface that have competency to depolarise negative charges cell membrane, in order to deliver encapsulated drugs or cosmetic functional ingredients into the skin. The cell viability studies verified the non-toxicity of both CT NPs samples towards human skin fibroblast cells. The CT/TPP and CT/CA NPs were shown to dominate the internalisation into these cells. Chitosan-acacia polymeric nanoparticles have an ability to penetrate and deliver the actives to the skin dermis layer. These results suggest that CT NPs could possibly be applied as innocuous carriers for active ingredients in cosmetics and skin drug delivery.

5. Acknowledgement:

The authors would like to thank Professor Phil Stephens (University of Cardiff, UK) for immortalised human dermal fibroblasts.

Reference

1. L. Mu, and R. Sprando. Application of Nanotechnology in Cosmetics. Pharm. Res.27(8), (2010), pp.1746-1749.

2. M. Bangale, Mitkare, and D. Sakarkar. Recent Nanotechnological Aspects In Cosmetics And Dermatological Preparations. Int. J. Pharm. and Pharm. Sci. 4(2), (2012), pp.88-97.

3. C. Appolonia Ibekwe, G. Modupe Oyatogun, T. AEsan, T. and M Oluwasegun . Synthesis and Characterization of Chitosan/Gum Arabic Nanoparticles for Bone Regeneration. Am. J. Mat. Sci. and Eng. 5(1), (2017), pp.28-36.

4. I. Aranaz, N. Acosta, C. Civera, B. Elorza, J. Mingo, C. Castro, M. Gandía. and A. Heras Caballero. Cosmetics and Cosmeceutical Applications of Chitin, Chitosan and Their Derivatives. Polymers, 10(2), (2018), p.213.

5. F. Larese Filon, M. Mauro, G. Adami,, M. Bovenzi and M. Crosera . Nanoparticles skin absorption: New aspects for a safety profile evaluation. Regulatory Toxicology and Pharmacology, 72(2), (2015), pp.310-322.

6. F. Rancan[1], Q. Gao, C. Graf, S.Troppens, S. Hadam, S. Hackbarth, C. Kembuan, U. Blume-Peytavi, E. Rühl, J. Lademann, A. Vogt. Skin penetration and cellular uptake of amorphous silica nanoparticles with variable size, surface functionalization, and colloidal stability. ACS Nano. 28; 6(8) (2012), pp 6829-42. doi: 10.1021/nn301622h. Epub 2012 Jul 19.

7. L.i W. Zhang , W. W. Yu, V. L. Colvin, N. A. Monteiro-Riviere. Biological interactions of quantum dot nanoparticles in skin and in human epidermal keratinocytes. Tox. and Appl. Pharmacol. 15;228(2), (2008), pp200-11. doi: 10.1016/j.taap.2007.12.022.

8. A. Jimtaisong, and N. Saewan.. Utilization of carboxymethyl chitosan in cosmetics. Int. J. of Cos. Sci. 36(1), (2013), pp.12-21.

9. J. Kumirska, M. Weinhold, J. Thömingand, P.Stepnowski. Biomedical Activity of Chitin/Chitosan Based Materials—Influence of Physicochemical Properties Apart from Molecular Weight and Degree of N-Acetylation. Polymers, 3(4), (2011), pp.1875-1901.

10. C. Qin, Y. Du, L. Xiao, Y. Liu,and H. Yu.. Moisture retention and antibacterial activity of modified chitosan by hydrogen peroxide. J. of App. Poly. Sci. 86(7), (2002), pp.1724-1730.

11. S. Sakulwech, N. Lourith, U. Ruktanonchai, and M. Kanlayavattanakul. Preparation and characterization of nanoparticles from quaternized cyclodextrin-grafted chitosan associated with hyaluronic acid for cosmetics. Asian J. Pharm. Sci. 13(5), (2018), pp.498-504.

12. A. Aliasghari, M. Khorasgani, S. Vaezifar, F. Rahimi, H. Younesi, and M. Khoroushi.. Evaluation of antibacterial efficiency of chitosan and chitosan nanoparticles on cariogenic streptococci: an in vitro study. Iranian J. Microb. 8(2), (2016), pp.93-100.

13. H. Abd El-Rehim, N. El-Sawy, E. Hegazy, E. Soliman, and A. Elbarbary . Improvement of antioxidant activity of chitosan by chemical treatment and ionizing radiation. Int. J. of Bio. Macromo. 50(2), (2012), pp.403-413. (13)
14. H. Misak, N. Zacharias., Z. Song, S. Hwang, P. Man, R. Asmatulu, R. Skin cancer treatment by albumin/5-Fu loaded magnetic nanocomposite spheres in a mouse model. J. of Biotech. 164 (1), (2013), pp 130–136.
15. R. PatiR. Mehta, S. Mohanty, A. Tech, M. Sangupta, B. Vaseeharan,C. Goswami, A. Sonawane. Topical application of zinc oxide nanoparticles reduces bacterial skin infection in mice and exhibits antibacterial activity by inducing oxidative stress response and cell membrane disintegration in macrophages. Nanomedicine: Nanotechnology, Biology and Medicine. 10(6), (2014), pp 1195-1208.
16. M. Aslam. M..Aqil, A.Abul Kalam, N.Yasmin, S.Asgar,. Application of Box–Behnken design for preparation of glibenclamide loaded lipid based nanoparticles: Optimization, in vitro skin permeation, drug release and in vivo pharmacokinetic study. J. of Mol. Liq. 219, (2016), pp. 897-908.
17. R. Al-Kassas, J. Wen A. Cheng, A. Kim, S. Liu, and J. Yu. Transdermal delivery of propranolol hydrochloride through chitosan nanoparticles dispersed in mucoadhesive gel. Carb. Polym. 153, (20-16), pp.176-186 DOI: 10.1016/j.carbpol.2016.06.096.
18. A. Nawaz, T. W. Wong. Chitosan-Carboxymethyl-5-Fluorouracil-Folate Conjugate Particles: Microwave Modulated Uptake by Skin and Melanoma Cells. J. of Inv. Dermatol. 138(11 (2018), pp 2412-2422. (18)
19. S. NtohogianV. Gavriliadou, E. Christodoulou, S. Nanaki, S. Lykidou, P. Naidis, L. Mischopoulou, P. Barmpalexis, N. Nikolaidis. and D. Bikiaris. . Chitosan Nanoparticles with Encapsulated Natural and UF-Purified Annatto and Saffron for the Preparation of UV Protective Cosmetic Emulsions. Molecules, 23(9), (2018), pp.2107. (17)
20. Q. Gan., T. Wang, C. Cochrane. and P. McCarron. Modulation of surface charge, particle size and morphological properties of chitosan–TPP nanoparticles intended for gene delivery. Collo. and Surf. B: Biointer. 44(2-3), (2005), pp.65-73. (20
21. G. Thandapani, and A. Sukumaran. Size optimization and in vitro biocompatibility studies of chitosan nanoparticles. Int. J. Bio. Macromol. 104, (2017), pp.1794-1806.
22. H. Trommer, H. Neubert. The examination of polysaccharides as potential antioxidative compounds for topical administration using a lipid model system. Int. J. Pharm. 14;298(1), (2005), pp. 153-63. doi: 10.1016/j.ijpharm.2005.04.024.
23. M. Avadi, A. Sadeghi, N. Mohammadpour, S. Abedin, F. Atyabi, R. Dinarvand, M. Rafiee-Tehrani. Preparation and characterization of insulin nanoparticles using chitosan and Arabic gum with ionic gelation method. Nanomedicine: Nanotechnology, Biology and Medicine 6. 2010; 58-63.

24. K. Joseph Akinluwade., G. Modupe Oyatogun., G. Alebiowu. and P. Popoola. Morphological analysis ofchitosan-acacia gum nanoparticles loaded and unloaded with cisplatin. Eur. J. Pharm. Med. Res. 5(6), (2018), pp.162-165.
25. C. Kiilll, H. Barud, S. Santagneli, S. Ribeiro, A. Silva, A. Tercjak, J. Gutierrez, A. Pironi. and M. Gremião.Synthesis and factorial design applied to a novel chitosan/ sodium polyphosphate nanoparticles via ionotropic gelation as an RGD delivery system. Carb. Polymers. 157, (2017), pp.1695-1702 DOI: 10.1016/j.carbpol.2016.11.053.
26. A. Rampino, M. Borgogna, P. Blasi.l. Chitosan nanoparticles: Preparation, size evolution and stability. Int. J. Pharm. 455(1-2), (2013), pp. 219-228.
27. E.Tang, M. Huang, and L. Lim. Ultrasonication of chitosan and chitosan nanoparticles. Int. J. Pharm., 265(1-2), (2003), pp.103-114. (24).
28. A. Martins, D. de Oliveira, A. Pereira., A. Rubiraand E. Muniz. Chitosan/TPP microparticles obtained by microemulsion method applied in controlled release of heparin. Int. J. Biol. Macromol. 51 (5), (2012), pp.1127-1133 DOI: 10.1016/j.ijbiomac.2012.08.032.
29. A. de Pinho Neves, C. Milioli, L. Müller, H. Riella, N. Kuhnen,. and H. Stulzer. Factorial design as tool in chitosan nanoparticles development by ionic gelation technique. Coll. and Surf. A: Physicochemical and Engineering Aspects, 445, (2014), pp.34-39 DOI: 10.1016/j.colsurfa.2013.12.058.
30. S. Loutfy, H. Alam El-Din, M. Elberry, N. AllamM. Hasaninand A. Abdellah. Synthesis, characterization and cytotoxic evaluation of chitosan nanoparticles: in vitro liver cancer model. Adv. Nat. Sci: Nanosci. and Nanotech. 7 (3), (2016), pp.035008 DOI: 10.1088/2043-6262/7/3/035008.
31. F. Abreu, N. Silva, M. Sipauba. Chitosan and gum arabic nanoparticles for heavy metal adsorption. Polímeros. 28(3), (2018), pp 231-238.
32. H. Abd-Allah., A. Kamel, and O. Sammour. Injectable long acting chitosan/tripolyphosphate microspheres for the intra-articular delivery of lornoxicam: Optimization and in vivo evaluation. Carb. Polym. 149, (2016), pp.263-273 DOI: 10.1016/j.carbpol.2016.04.096. (34)
33. J. Azevedo, R. Sizilio, M. Brito, A. Costa, M. Serafini, A. Araújo, M. Santos, A. Lira and R. Nunes.Physical and chemical characterization insulin-loaded chitosan-TPP nanoparticles. J. Therm. Anal. Calorim. 106 (3), (2011), pp.685-689 DOI: 10.1007/s10973-011-1429-5.
34. Z. Wang, R. Zeng, M. Tuand J. Zhao. Synthesis, characterization of biomimetic phosphorylcholine-bound chitosan derivative and in vitro drug release of their nanoparticles. J. Appl. Polym. Sci. 128 (1), (2012), pp.153-160 DOI: 10.1002/app.38151.
35. H. Yadav, A. Almokdad, S. Shaluf, and M. Debe. Chapter 17 - Polymer-Based Nanomaterials for Drug-Delivery Carriers. In Mohaptra, S., Ranjan, S., Dasgupta, N., Mishra,

R. and Thomas, S. (ed.) Nanocarriers for Drug Delivery, Amsterdam: Elsevier pp.531-556 [Accessed 20th August 2019].
36. S. H. Othman,N. Kechik , R. A. Shapi'i,R. A. Talib ,and I. Tawakkal. Water Sorption and Mechanical Properties of Starch/Chitosan Nanoparticle Films. J. Nanomat. (2019). https://doi.org/10.1155/2019/3843949.
37. Q. Lei, J. Pan, J. Bao, Z. Huang, and Y. Zhang.Analysis and modeling of moisture sorption behaviour for antimicrobial composite protein films. Biom. Mat. Eng. 24(6), (2014), pp. 1969–1978..
38. E. Szymańska, K. Winnicka.. Stability of Chitosan—A Challenge for Pharmaceutical and Biomedical Applications. Marine Drugs. 13(4), (2015), 1819-1846. Available from:https://www.ncbi.nlm.nih.gov/pmc/articles/PMC4413189/
39. K. Nolan, E. Marmur. Moisturizers: reality and the skin benefits. Dermatol. Ther.25(3), (2012), PP. 229-33. doi: 10.1111/j.1529-8019.2012.01504.x.
40. T. Mosmann. Rapid colorimetric assay for cellular growth and survival: application to proliferation and cytotoxicity assays. J. Immunol. Meth. 65, (1983), pp. 55-63.
41. H. Jee. Kim, J. Leeand H. Lee. Release Properties and Cellular Uptake in Caco-2 Cells of Size-Controlled Chitosan Nanoparticles. J. Agricul. Food Chem. 65(50), (2017), pp.10899-10906.
42. P. Foroozandeh, and A. Aziz. (2018). Insight into Cellular Uptake and Intracellular Trafficking of Nanoparticles.. Nanosc. Res. Lett. 13(339), (2018). https://doi.org/10.1186/s11671-018-2728-6
43. A. Summerfield, F. Meurens, M. Ricklin. The immunology of the porcine skin and its value as a model for human skin. Mol. Imm. 66(1), (2015),pp. 14-21. Available from: https://www.ncbi.nlm.nih.gov/pubmed/25466611
44. C. Mate, S. Mishra. Exploring the Potential of Moi Gum for Diverse Applications: A Review. J. Polym. and Enviro. 28, (2020), pp. 1579-1591.

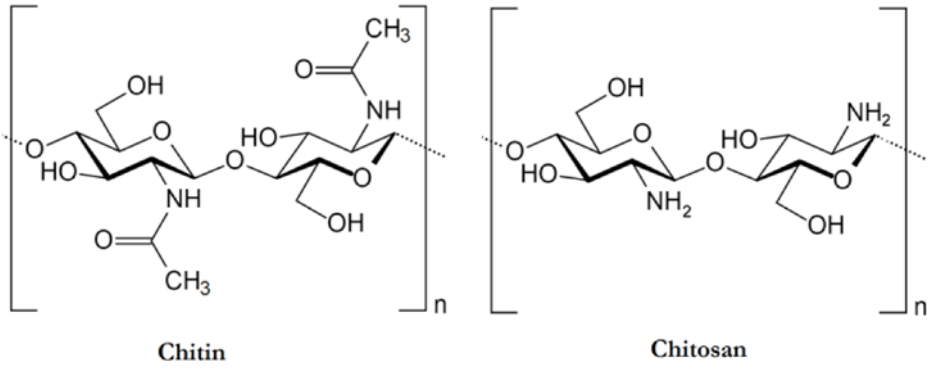

Figure 1.a: Differences in chitin and chitosan chemical structures

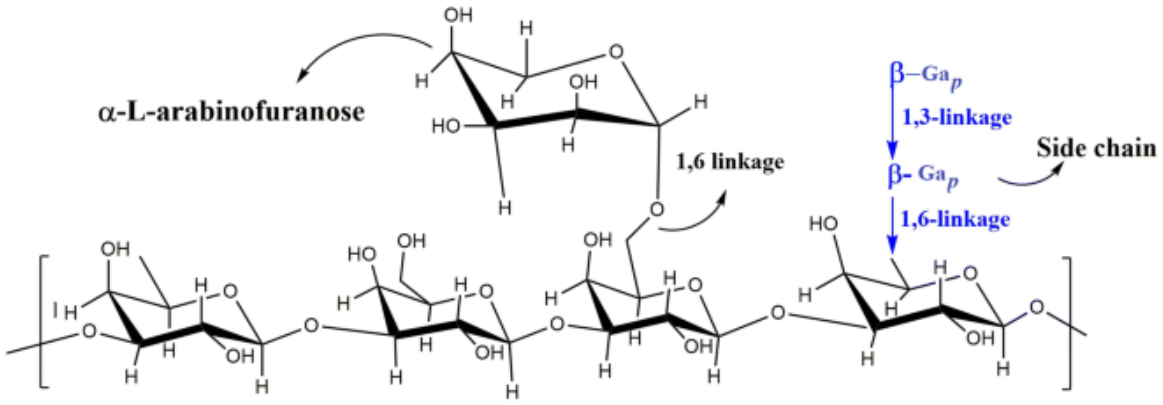

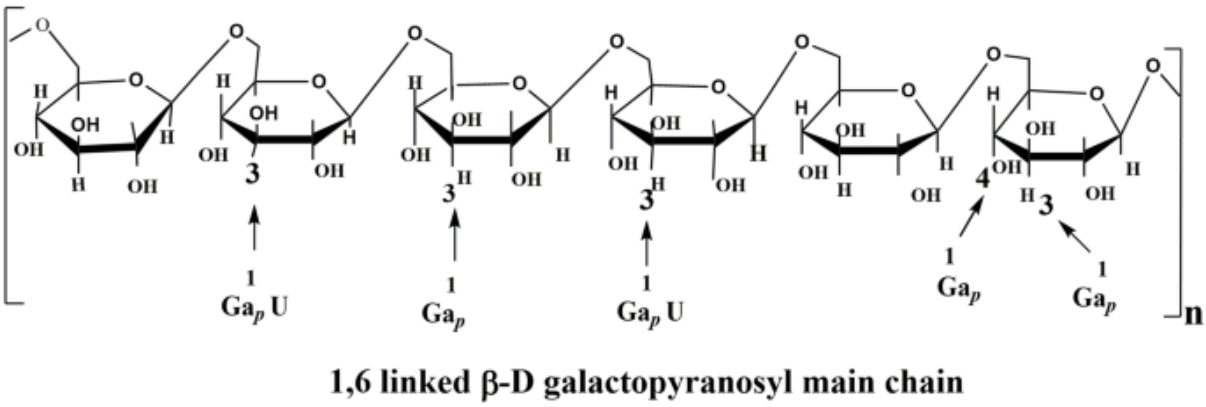

Figure 1.b: The chemical structure of acacia [44].

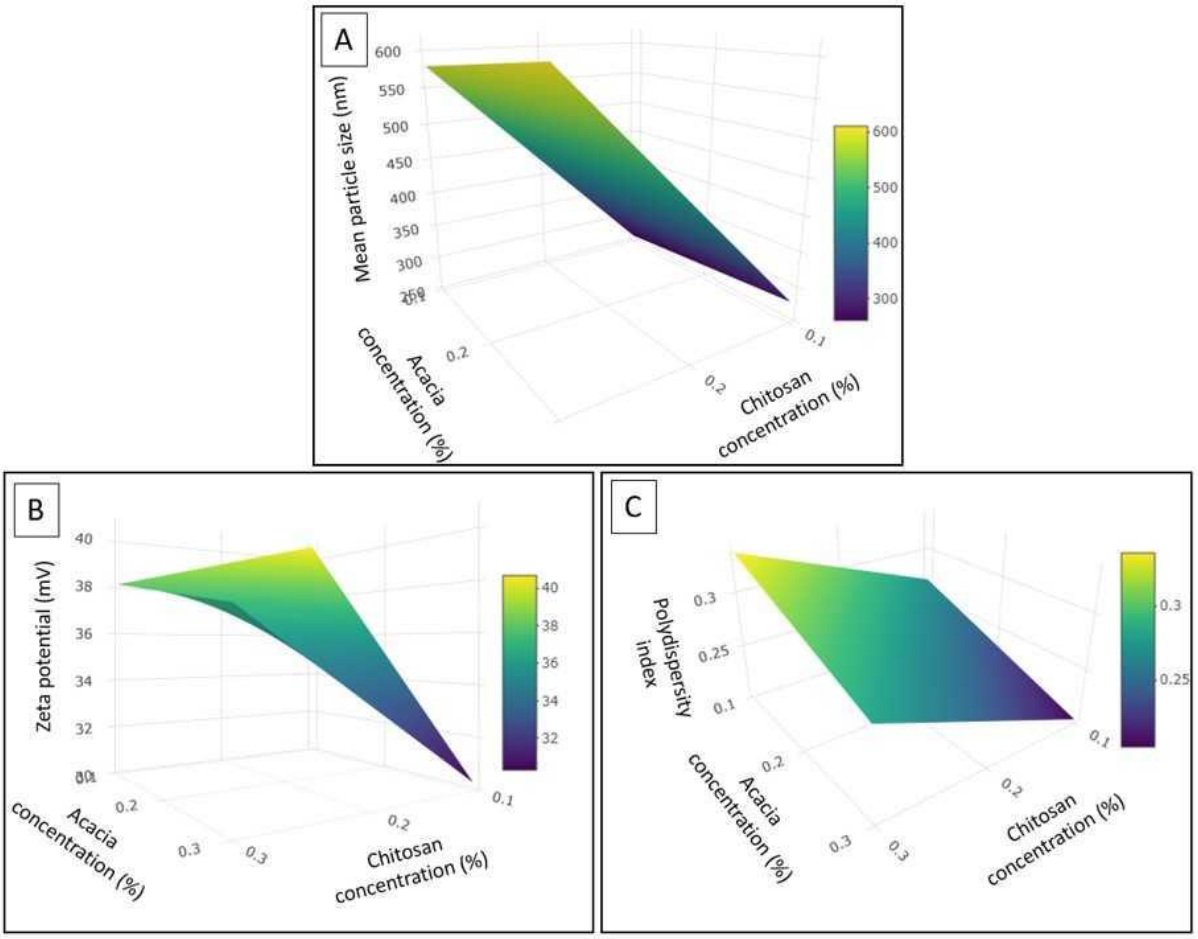

Figure 2: Surface response plot of the effect of chitosan and acacia concentrations on: (A) nanoparticle size; (B) zeta potential; (C) polydispersity index.

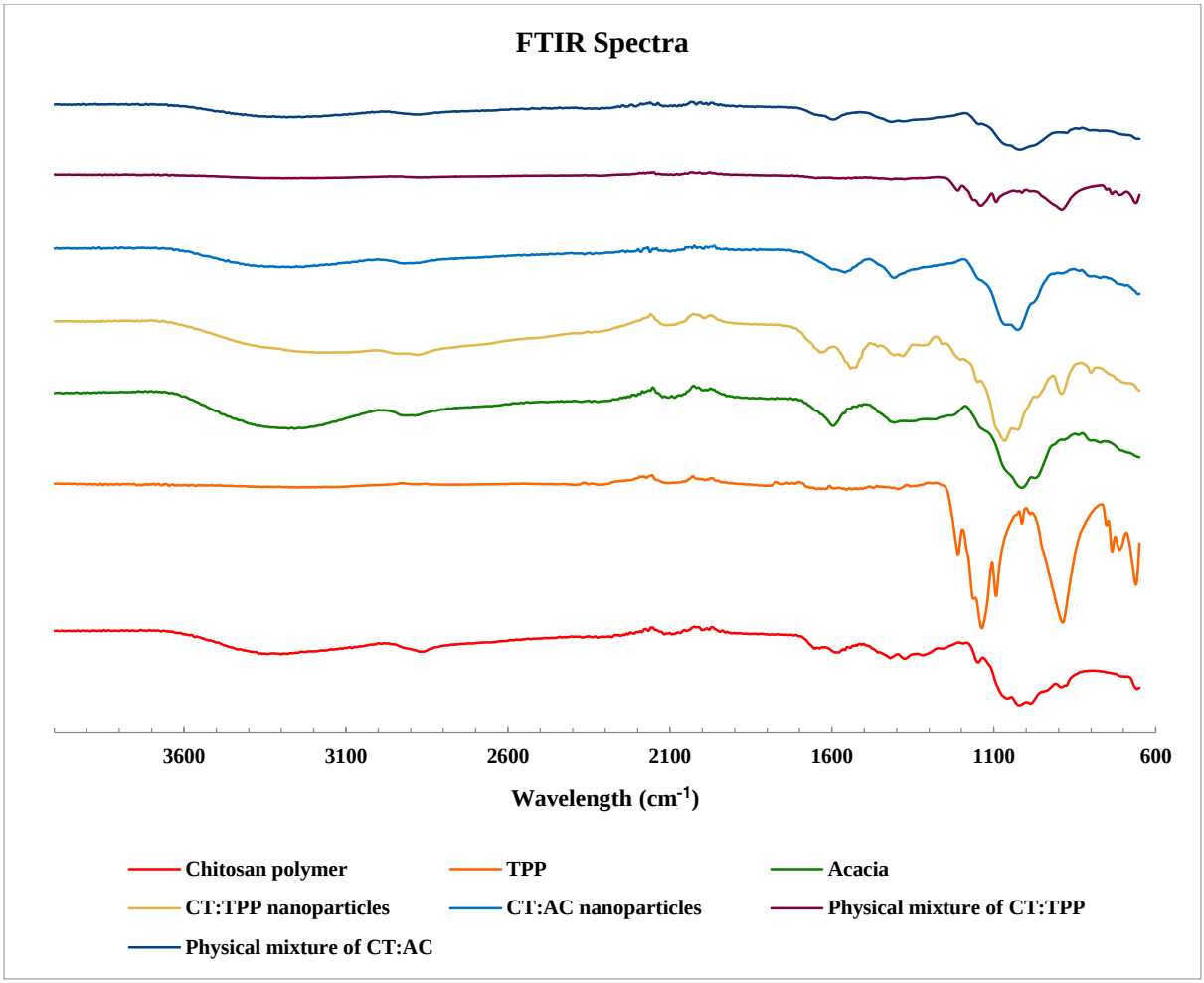

Figure 3: FTIR spectra analysed from the wavelength of 4000 to 600cm-1.

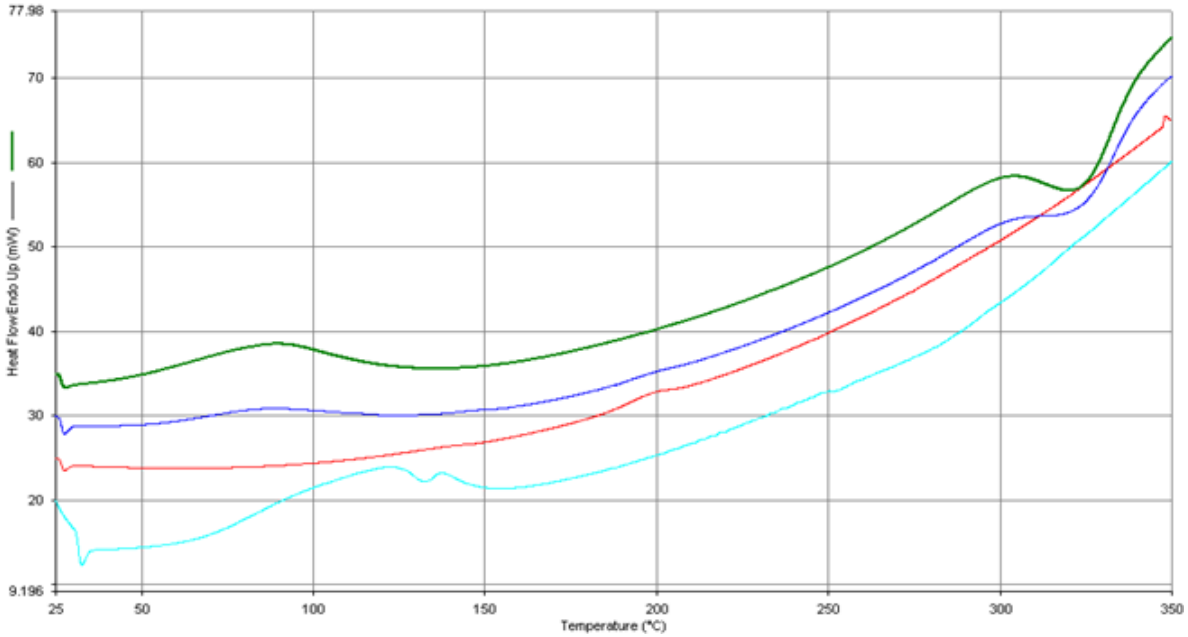

Figure 4.a DSC thermograms of Chitosan (green), a 1:1 physical mixture of Chitosan and TPP (dark blue), TPP (red) and nanoparticles (light blue).

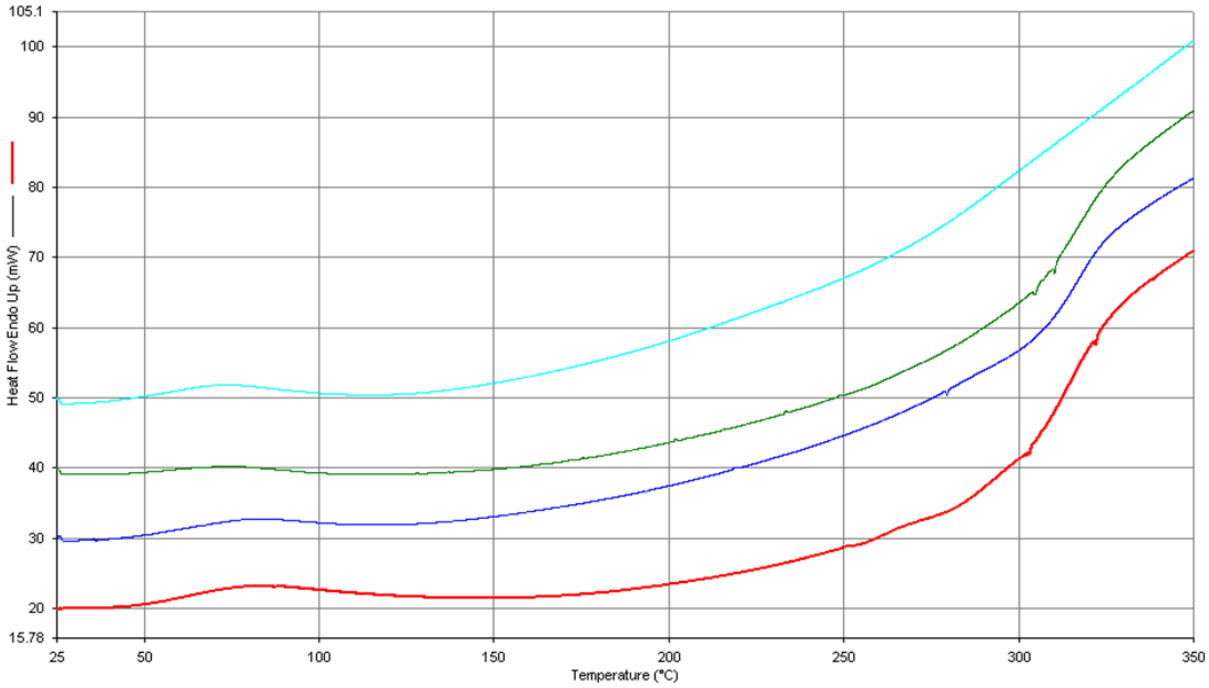

Figure 4.b DSC thermo-grams obtained from 25 to 350 °C at 10 °C/min for acacia (red), chitosan polymer (blue), 1:1 physical mixture of chitosan to acacia (green), and the freeze-dried nanoparticles (teal).

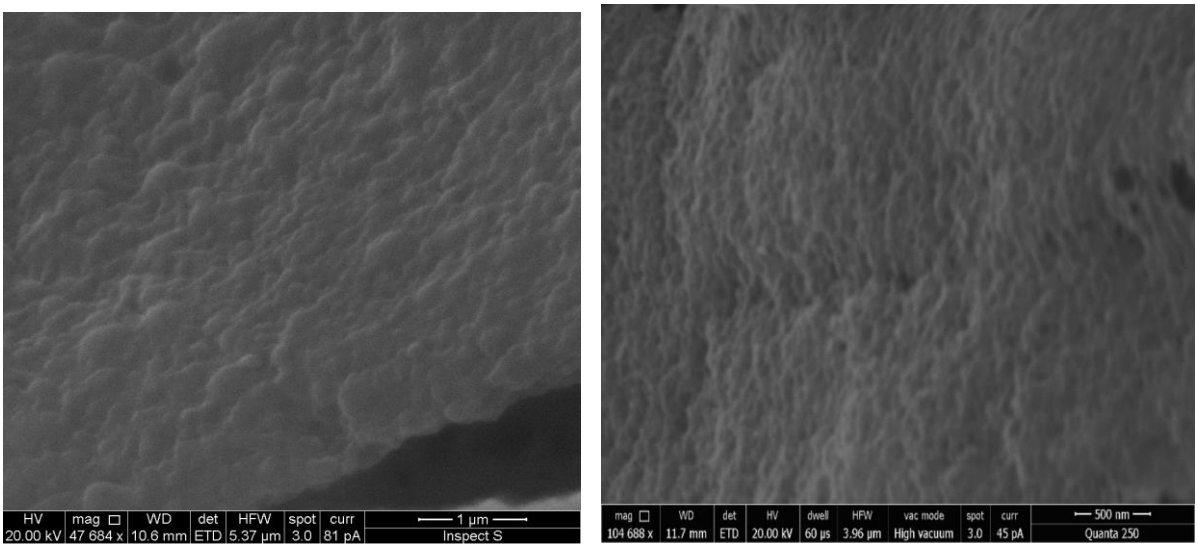

Figure 5.a SEM micrographs taken at 20.00 kV showing freeze-dried polymeric nanoparticles yielded from CT/ AC (left) and CT/TPP nanoparticles (right).

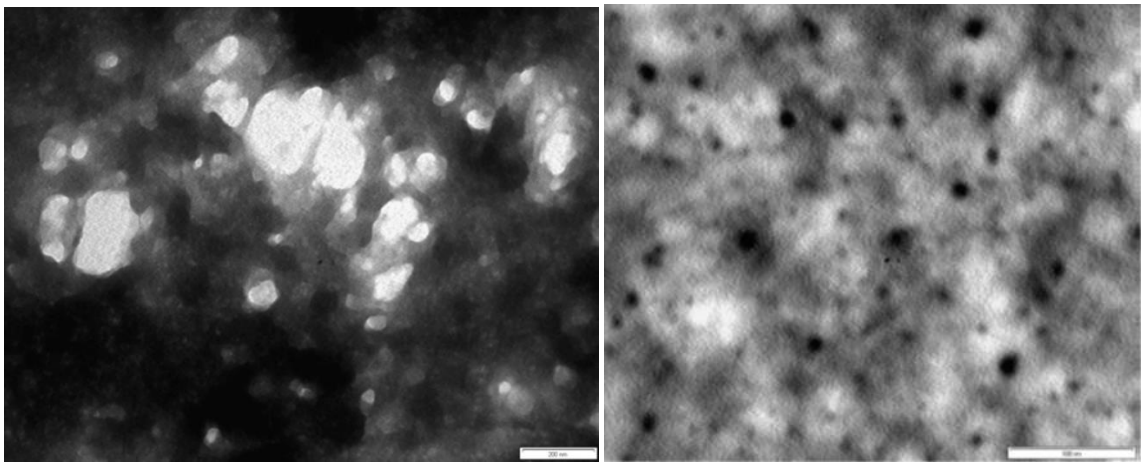

Figure 5.b. TEM images showing wet polymeric nanoparticles yielded from CT:AC (right) and CT:TPP (left).

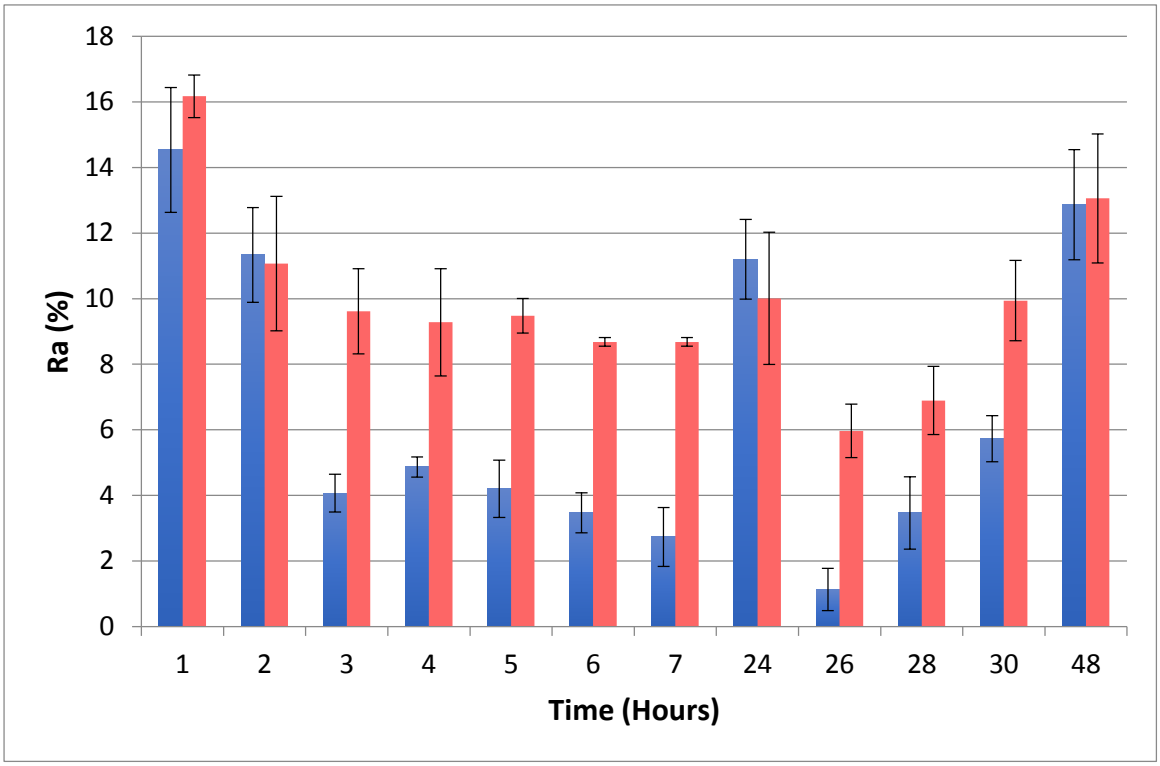

Figure 6.a. Histogram depicting the moisture absorption (Ra) of CT NPs over 48 hours where blue is CT NPs prepared using TPP and red is CT NPs prepared using acacia.

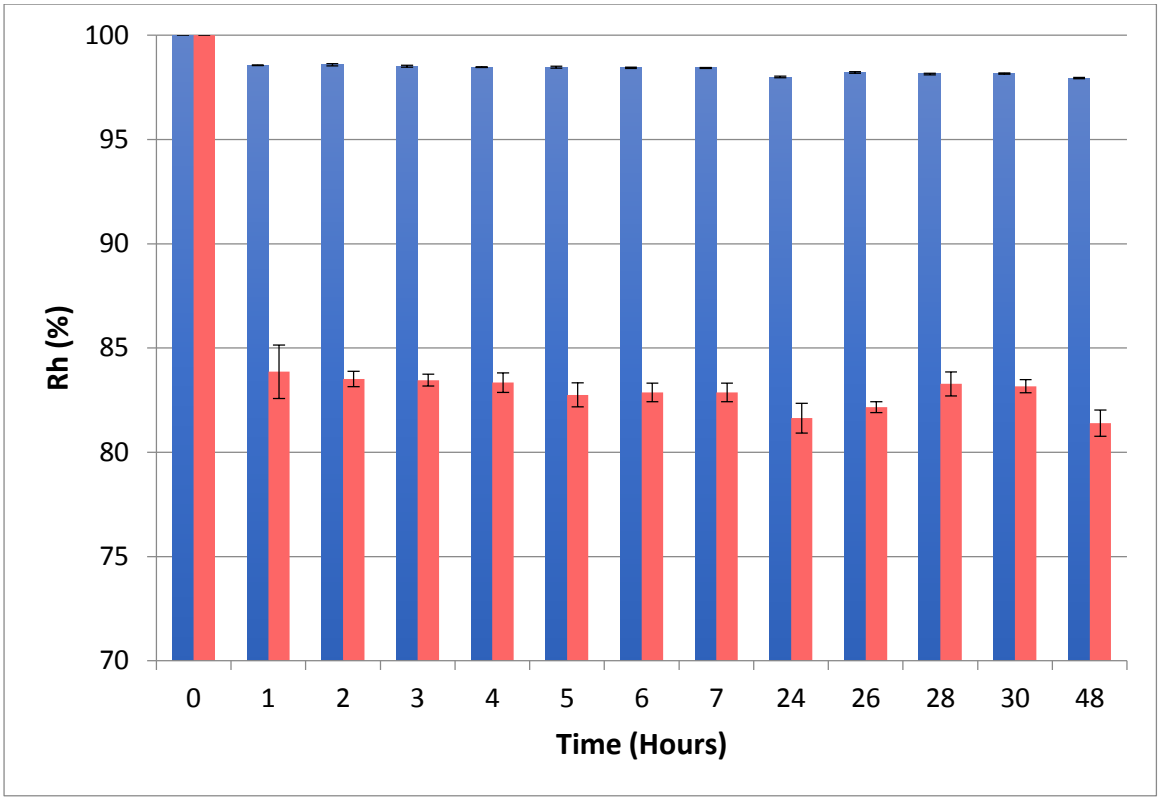

Figure 6.b. Histogram depicting the moisture retention (Rh) of CT NPs over 48 hours where blue is CT NPs prepared using TPP and red is CT NPs prepared using acacia.

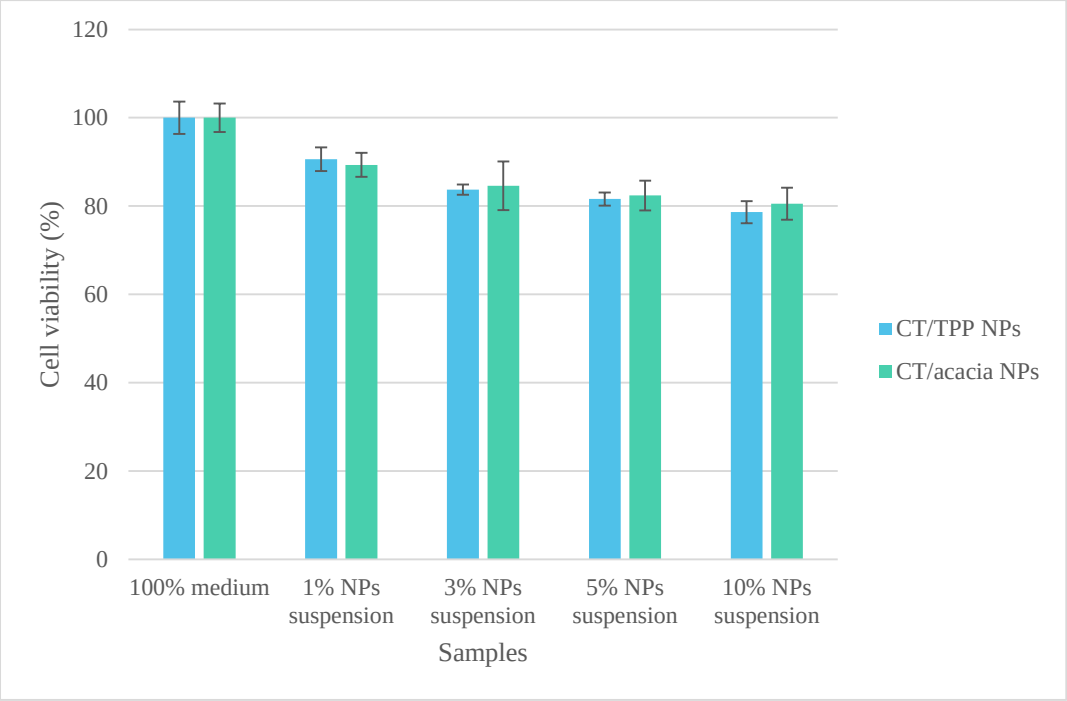

Figure 7– Cell viability measured by MTT assay after 48-hour exposure of fibroblast cells to CT/TPP NPs, CT/AC NPs.

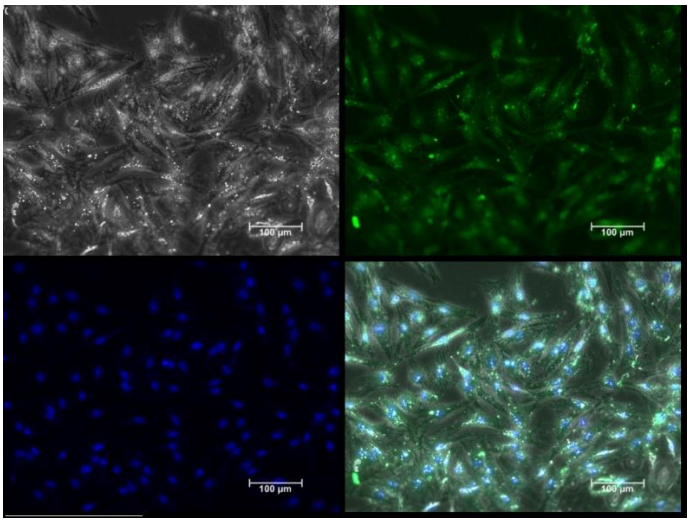

Figure 8.a– Live cell images of fibroblast cells after incubating with FSS loaded CT/TPP NPs (x20 magnification).

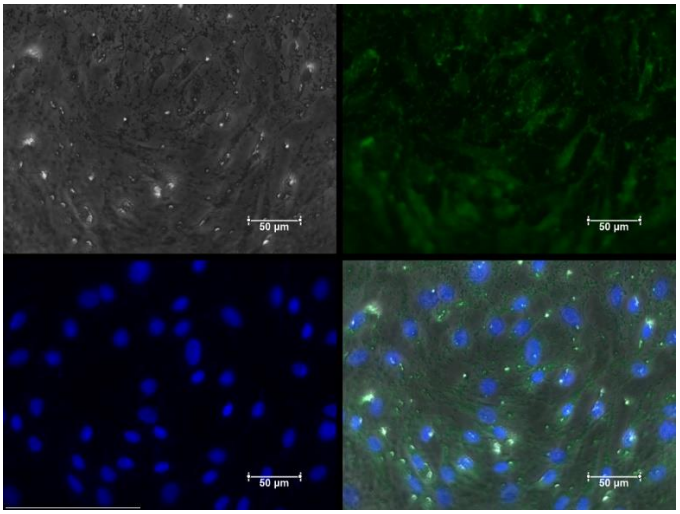

Figure 8.b– Live cell images of fibroblast cells after incubating with FSS loaded CT/acacia NPs (x20 magnification).

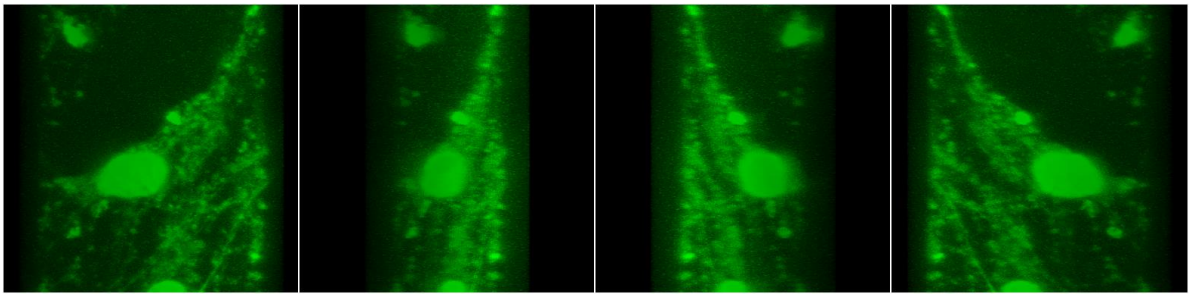

Figure 8.c– 3D images of a single fibroblast cell incubated with FSS loaded CT/acacia NPs

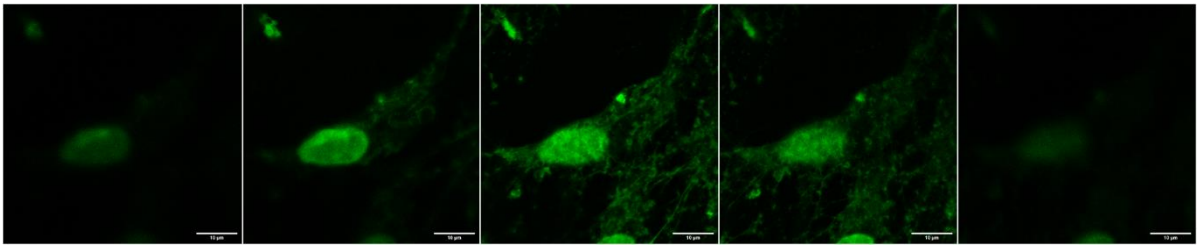

Figure 8.d– Z-stack images of a single fibroblast cell incubated with FSS loaded CT/acacia NPs

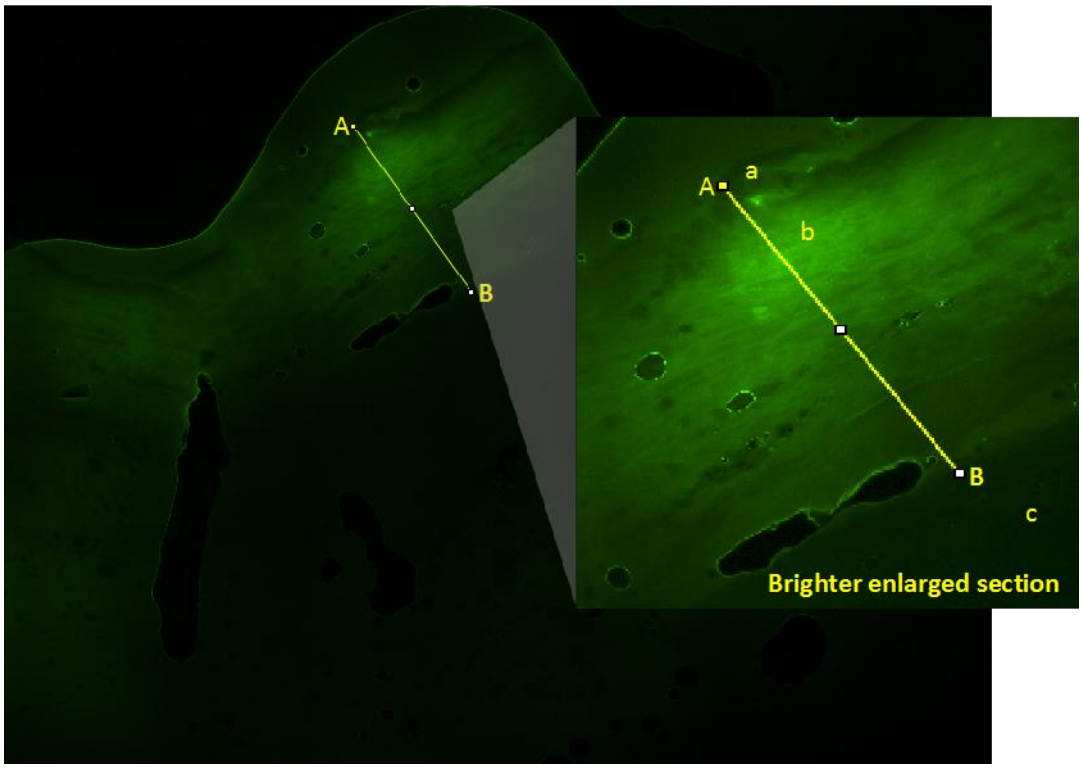

Figure 9.a. Porcine ear skin penetration imaging from confocal microscopy with the line profile position AB shown. Histology of porcine ear skin from the enlarged section: (a) Epidermis; (b) dermis; (c) subcutaneous tissues.

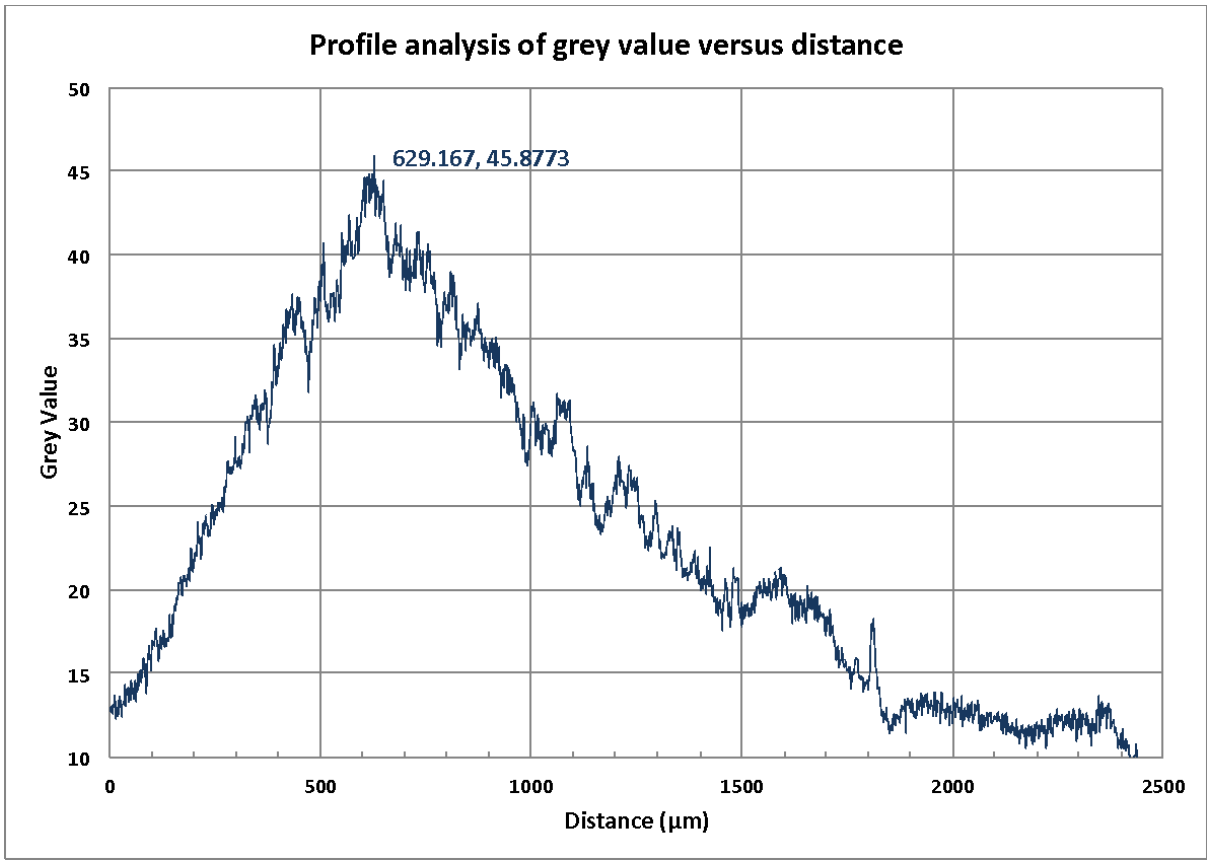

Figure 9.b. Line profile analysis from the position shown in Figure 10.a with Fiji Image J.

Table 1: Initial 3 level factorial design, providing the lower, medium and upper level values for each variable.

Variables	**Levels**		
	Low level (-1)	Medium Level (0)	High level (+1)
Chitosan concentration X_1	0.1%	0.2%	0.3%
Acacia ConcentrationX_2	0.1%	0.2%	0.3%

Table 2: Experimental and predicted results in terms of mean particle size (Z-Ave), zeta potential (ZP), and polydispersity index (PDI) for 10 different formulations, with the results from Formulation 10 as the analytical test data.

Exp	Conc. (%)		Results					
Nº	CT	Acacia	ZP*±S.D. exp.** (mV)	ZP pred.*** (mV)	Z-Ave ± S.D. exp. (nm)	Z-Ave pred. (nm)	PDI ± S.D. exp.	PDI pred.
F1	0.1	0.1	38.467 ± 0.153	40.664	285.333 ± 6.824	260.521	0.295 ± 0.012	0.269
F2	0.1	0.2	34.767 ± 0.351	35.489	291.500 ± 10.417	270.891	0.233 ± 0.012	0.237
F3	0.1	0.3	27.833 ± 0.404	30.314	303.967 ± 10.616	281.260	0.223 ± 0.025	0.205
F4	0.2	0.1	41.767 ± 0.208	39.389	370.733 ± 6.702	420.224	0.279 ± 0.010	0.303
F5	0.2	0.2	41.933 ± 0.666	36.456	391.567 ± 8.199	433.052	0.226 ± 0.025	0.273
F6	0.2	0.3	36.467 ± 3.499	33.522	400.600 ± 7.908	445.880	0.233 ± 0.042	0.243
F7	0.3	0.1	36.333 ± 0.404	38.114	602.600 ± 13.432	579.927	0.347 ± 0.013	0.336
F8	0.3	0.2	35.867 ± 0.551	37.422	620.100 ± 5.027	595.213	0.334 ± 0.052	0.308
F9	0.3	0.3	34.667 ± 0.924	36.731	631.067 ± 11.102	610.500	0.284 ± 0.035	0.281
F10	0.25	0.25	36.067 ± 0.643	36.033	520.733 ± 9.928	521.161	0.332 ± 0.035	0.276

***Zeta Potential **experimental ***predicted**

Table 3: Student's *t*-test analysis of the standard error, *t* statistic, and *p*-value for mean particle size (Z-Ave), zeta potential (ZP), and the polydispersity index (PDI).

	β_0	β_1	β_2	β_{12}
ZP	49.356	-35.167	-74.167	224.167
Standard error	4.221	19.538	19.538	90.443
***t* statistic**	11.694	-1.800	-3.796	2.479
***p*-value**	<0.001	0.085	0.001	0.021
Z-Ave	92.910	1572.440	79.110	245.830
Standard error	48.280	223.500	223.500	1034.580
***t* statistic**	1.924	7.036	0.354	0.238
***p*-value**	0.067	<0.001	0.727	0.814
PDI	0.271	0.308	-0.348	0.242
Standard error	0.048	0.221	0.221	1.022
***t* value**	5.677	1.396	-1.575	0.236
***p*-value**	<0.001	0.176	0.129	0.815

Table 4: ANOVA analysis of residual standard error, multiple R-squared, adjusted R-squared, *F*-value, and *p*-value for mean particle size (Z-Ave), zeta potential (ZP), and the polydispersity index (PDI).

	Residual standard error	**Multiple R-squared**	**Adjusted R-squared**	***F*-statistic**	***p*-value**
ZP	3.133	0.507	0.443	7.878	<0.001
Z-Ave	35.840	0.942	0.934	123.600	<0.001
PDI	0.035	0.576	0.520	10.400	<0.001

Table 5: The characteristics of fresh chitosan NPs prepared by 0.2% w/v of LMW, MMW and HMW chitosan with two cross-linkers (0.05% w/v) at ambient temperature by ionic gelation method (Mean ± SD, n=3)

	CT/TPP NPs			CT/acacia NPs		
	Particle size (nm)	PDI	Zeta potential (mV)	Particle size (nm)	PDI	Zeta potential (mV)
LMW chitosan	198.50±14.72	0.66±0.11	27.27±1.18	249.90±10.04	0.25±0.03	29.90±2.19
MMW chitosan	251.57±13.74	0.49±0.02	33.77±0.96	284.37±3.65	0.34±0.05	32.87±0.98
HMW chitosan	407.67±29.25	0.79±0.36	25.77±1.87	304.83±29.61	0.30±0.07	32.57±0.90

Table 6: Bands of interest from the FTIR Spectra shown in *Figure 9.*

Sample	Band	Assignment
Chitosan	1023 and 1058cm^{-1}	C – O stretching vibration
	1149cm^{-1}	C – N stretching vibration
	1377cm^{-1}	C – H bending vibration (CH_2CH_3)
	1420cm^{-1}	C-H asymmetric deformation of acetamide
	1589cm^{-1}	N – H bending vibration of amide II
	1653cm^{-1}	C = O stretching vibration of amide group I (-CONH)
	2864cm^{-1}	C – H stretching vibration
	3345cm^{-1}	O – H (aromatic H – bond) stretching vibration overlapped with N – H stretching vibration
TPP	889cm^{-1}	P – O – P asymmetric stretching
	1094cm^{-1}	PO_3 groups stretching vibration (symmetric and asymmetric)
	1136cm^{-1}	PO_2 groups stretching vibration (symmetric and asymmetric)
	1209cm^{-1}	P = O stretching vibration
Acacia	1023cm^{-1}	C – OH stretching vibration
	1407cm^{-1}	Carboxylic ion axial asymmetric stretching
	1595cm^{-1}	O=C-O symmetric stretching
CT NPs (TPP)	1541cm^{-1}	N – O – P stretching vibration
CT NPs (Acacia)	1400 to 1600cm^{-1}	Overlapping of COO^- main stretching and charged amino (NH_3^+) asymmetrical bending

Conflict of interest:

The authors declare no potential conflict of interests.